Integrating Interpretable Machine Learning and Multi-omics Systems Biology for Personalized Biomarker Discovery and Drug Repurposing in Alzheimer's Disease

Mohammadsadeq Mottaqi[1], Pengyue Zhang[2*], Lei Xie[1,3,4,5,6*]

[1] Ph.D. Program in Biochemistry, The Graduate Center, The City University of New York, New York, 10016, NY, USA

[2] Department of Biostatistics and Health Data Science, Indiana University School of Medicine, Indianapolis, 46202, IN, USA

[3] Center for Drug Discovery and Department of Pharmaceutical Sciences, Northeastern University, Boston, 02115, MA, USA

[4] Department of Computer Science, Hunter College, The Graduate Center, The City University of New York, New York, 10016, NY, USA

[5] Ph.D. Program in Computer Science, The Graduate Center, The City University of New York, New York, 10016, NY, USA

[6] Helen & Robert Appel Alzheimer's Disease Research Institute, Feil Family Brain & Mind Research Institute, Weill Cornell Medicine, Cornell University, New York, 10065, NY, USA

Keywords: Computational Biology, GWAS, Transcriptomics, Biological Network, Personalized Medicine, Drug Repurposing

Abstract

Background

Alzheimer's disease (AD) is a complex neurodegenerative disorder with substantial molecular variability across different brain regions and individuals, hindering therapeutic development. This study introduces PRISM-ML, an interpretable machine learning (ML) framework integrating multiomics data to uncover patient-specific biomarkers, subtissue-level pathology, and drug repurposing opportunities.

Methods

We harmonized transcriptomic and genomic data of three independent brain studies containing 2105 post-mortem brain samples (1363 AD, 742 controls) across nine tissues. A Random Forest classifier with SHapley Additive exPlanations (SHAP) identified patient-level biomarkers. Clustering further delineated each tissue into subtissues, and network analysis revealed critical "bottleneck" (hub) genes. Finally, a knowledge graph-based screening identified multi-target drug candidates, and a real-world pharmacoepidemiologic study evaluated their clinical relevance.

Results

We uncovered 36 molecularly distinct subtissues, each defined by a set of associated unique biomarkers and genetic drivers. Through network analysis of gene-gene interactions networks, we highlighted 262 bottleneck genes enriched in synaptic, cytoskeletal, and membrane-associated processes. Knowledge graph queries identified six FDA-approved drugs predicted to target multiple bottleneck genes and AD-relevant pathways simultaneously. One candidate, promethazine, demonstrated an association with reduced AD incidence in a large healthcare dataset of over 364000 individuals (hazard ratios ≤ 0.43; $p < 0.001$). These findings underscore

the potential for multi-target approaches, reveal connections between AD and cardiovascular pathways, and offer novel insights into the heterogeneous biology of AD.

Conclusions
PRISM-ML bridges interpretable ML with multi-omics and systems biology to decode AD heterogeneity, revealing region-specific mechanisms and repurposable therapeutics. The validation of promethazine in real-world data underscores the clinical relevance of multi-target strategies, paving the way for more personalized treatments in AD and other complex disorders.

Background

Alzheimer's disease (AD) is characterized by progressive brain shrinkage, leading to symptoms such as memory loss, dementia, and language difficulties. This neurodegenerative disorder is marked by the accumulation of amyloid-beta plaques and tau protein tangles, which disrupt neuronal communication and contribute to the cognitive decline observed in patients (1). Despite its significant societal impact, the molecular mechanisms underlying AD remain incompletely understood, posing a substantial challenge for developing effective therapies. Currently, treatments focus primarily on symptom management rather than altering disease progression, as existing medications do not address the underlying disease mechanisms (2).

Advancements in understanding AD have been driven by leveraging extensive experimental research and patient data, which provide insights into the complex signaling pathways that drive disease progression. However, significant challenges persist in diagnosing and understanding AD due to its complex biological nature (Zhang et al., 2024). Traditional bioinformatics methods, such as differential gene expression analysis, often fail to capture the intricate, predominantly nonlinear patterns in biological data and the heterogeneity of AD. Moreover, studies often focus on single omics data types in isolation, which limits our understanding of the systemic nature of the disease (3). While current therapeutic approaches typically target a single molecule or a pathway, the complex pathophysiology of AD demands a more comprehensive strategy. Moreover, although Machine Learning (ML) and deep learning have shown promise in analyzing biological data, the opaque nature of these models, the "black box", often hinders their practical utility in elucidating disease mechanisms (4).

To overcome these challenges, we have developed a comprehensive data mining framework, PRISM-ML (PRecision-medicine using Interpretable Systems and Multiomics with Machine Learning), that integrates multiple omics data and combines interpretable ML with systems biology to elucidate the molecular mechanisms of AD for individual patients. By combining bulk RNA sequencing (RNA-seq) transcriptomics data with Genome-wide Association Study (GWAS) data from the same patient and control cohort, we have identified patient-level and subtissue-

specific biomarkers and genetic markers. This approach has enabled the construction of biologically meaningful subtissue-specific gene-gene interaction networks. Employing a Random Forest classification model with a leave-one-patient-out cross-validation (LOOCV) strategy and utilizing SHapley Additive exPlanations (SHAP).

Finally, our framework addresses the interpretability challenges common in ML while maintaining high predictive accuracy. By revealing primary cellular dysregulations and identifying critical intermediate message-passing genes within pathways, our research ultimately identified six multi-target repurposed drugs predicted to strongly and effectively interact with multiple network hub genes. One of drug candidates, promethazine is associated with a markedly reduced risk of AD (hazard ratios (HRs) ≤ 0.43; $p < 0.001$) in a large cohort from real-world healthcare data, supporting the validity of our approach.

Through network analysis that connects different omics layers, we provide a systems-level understanding of AD pathology, paving the way for more effective therapeutic precision-medicine treatment strategies. The subsequent sections of this manuscript will detail our methodologies, findings, and the implications of our integrated multiomics approach to study AD.

Results

1. Overview of the PRISM-ML Framework

In this study, we introduce PRISM-ML (PRecision-medicine using Interpretable Systems and Multiomics with Machine Learning) as a framework for analyzing AD through multiomics and systems-level lens (Fig. 1). By integrating transcriptomic and genomic data from over 2,100 post-mortem samples across nine brain tissues, PRISM-ML illuminates patient-specific molecular features and regional disease heterogeneity. Its combination of interpretable ML and systems biology pinpoints dysregulated pathways and enables systematic exploration of potential therapeutics via drug repurposing.

Conceptually, PRISM-ML follows four major steps. First, a Random Forest classifier (optimized and explained via SHAP (5)), was used to identify high-impact biomarkers distinguishing AD samples from control samples on an individual patient basis. Second, clustering segments each brain region into multiple “subtissues,” capturing local molecular patterns. Third, these subtissue-level biomarkers, combined with AD-associated variants, form gene-gene interaction networks that reveal “bottleneck” genes critical for AD-related pathways. Finally, a knowledge graph

approach highlights FDA-approved drugs that target these bottleneck genes, identifying candidates capable of influencing multiple disease-relevant pathways.

This multi-pronged strategy yields several key insights. We identified 36 distinct subtissues and 262 critical bottleneck genes—central mediators of AD pathology—enriched in genes related to synaptic transmission, cytoskeletal regulation, and extracellular matrix organization. Amonf the six predicted multi-target drugs, promethazine demonstrated a 62% reduction in AD risk in an independent pharmacoepidemiologic dataset, validating its clinical potential.

PRISM-ML advances precision medicine by unifying patient-specific biomarkers, subtissue-level pathology, and multi-target drug discovery into a single pipeline. Its interpretable design addresses the "black box" limitations of conventional ML, whereas its systems biology approach uncovers shared mechanisms between AD and comorbidities such as cardiovascular diseases. This framework establishes a blueprint for studying complex diseases, emphasizing actionable therapeutic insights over isolated molecular signatures.

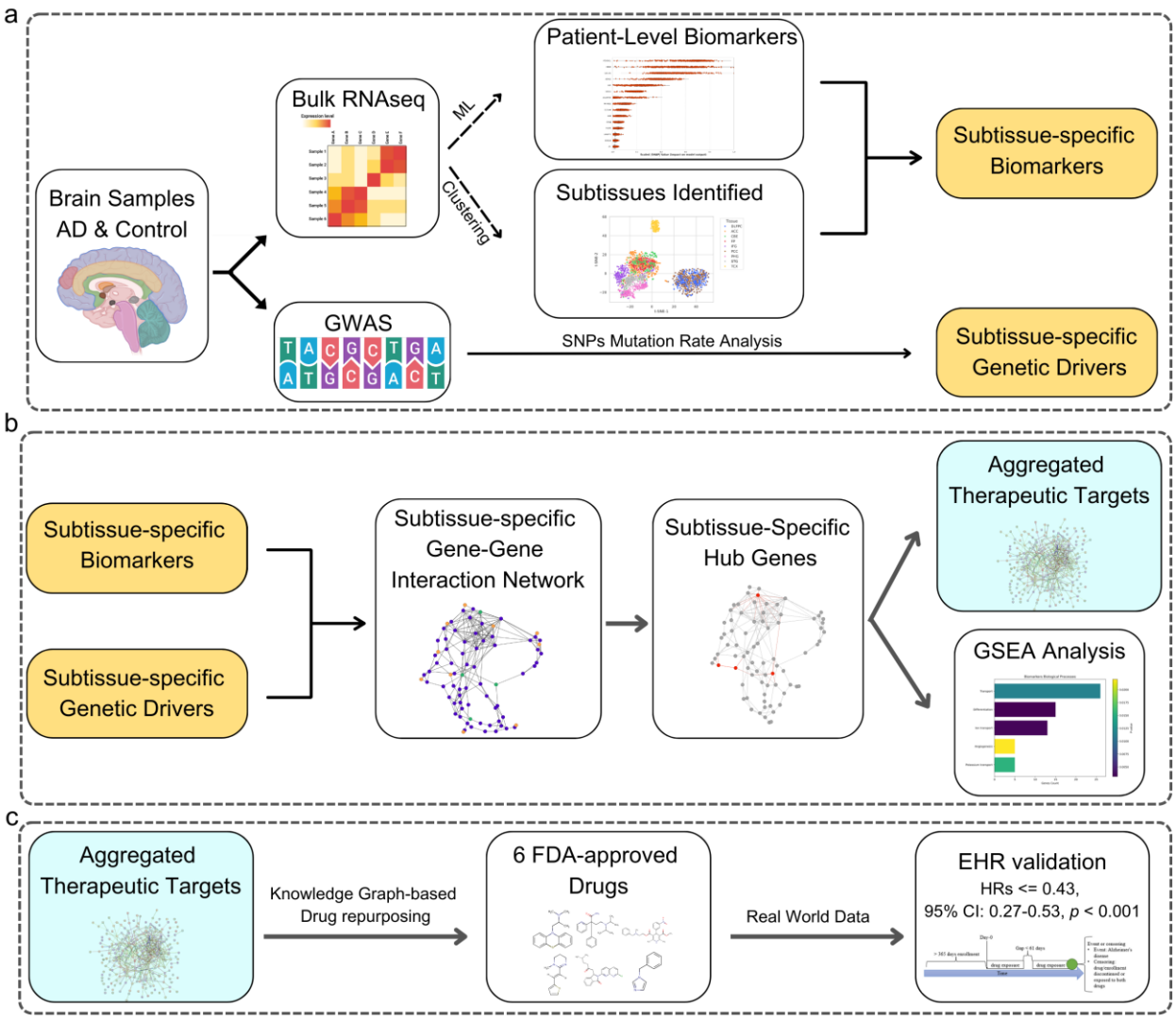

Figure 1. PRISM-ML: integrating systems biology, multiomics, machine learning for Alzheimer's disease drug repurposing.

(a) Multiomics integration and subtissue identification: Bulk RNA-seq and GWAS data from 2,105 post-mortem brain samples (1,363 AD patients, 742 controls) across nine tissues were harmonized. A Random Forest classifier with SHAP analysis identified 175 patient-specific unique biomarkers per sample on average. Unsupervised clustering stratified each tissue into four molecularly distinct subtissues (36 in total). Subtissue-specific biomarkers—high-impact genes shared across samples within each subtissue cluster—were derived by intersecting patient-level biomarker sets. Mutation rate analysis of AD-associated SNPs revealed subtissue-specific genetic drivers.

(b) Subtissue-specific networks and bottleneck genes: Subtissue-specific gene-gene interaction networks connect biomarkers and genetic drivers via critical intermediate "message-passing" genes. Topological metrics (e.g., betweenness centrality) prioritized 262 high-centrality bottleneck genes enriched in synaptic transmission, ion transport, and extracellular matrix organization.

(c) Drug repurposing and real-world validation: Knowledge-graph screening flags six FDA-approved drugs (e.g., promethazine, Disopyramide) that target multiple bottleneck genes. In a cohort of 364733 individuals, promethazine use was associated with a significantly reduced AD risk (HRs ≤ 0.43; $p < 0.001$).

2) PRISM-ML Identifies Patient-level AD Biomarkers

First, we compiled a multiomics dataset by merging matched bulk RNA-sequencing and genome-wide association study (GWAS) data from the same donors in three large-scale AD brain tissue studies: the Religious Orders Study and Rush Memory and Aging Project (ROSMAP) (6), The Mount Sinai Brain Bank (MSBB) (7), and the Mayo RNA-seq study (MAYO) (8). This integration yielded 2,105 post-mortem brain tissue samples—1,363 classified as AD patients and 742 as controls—originating from 307 males and 528 females (Table 1). Each sample came from one of nine distinct brain tissues (details in *Methods*). By ensuring that both transcriptomic and genomic data were derived from the same individuals, this harmonized dataset provides a robust foundation for downstream analyses, capturing patient-level molecular variation across diverse brain tissues. Figure 2a presents a t-Distributed Stochastic Neighbor Embedding (t-SNE) plot visualizing the distribution of total samples in the data.

To identify patient-specific biomarkers underlying AD heterogeneity, we analyzed the gene expression profiles of brain samples. We then trained a Random Forest classifier—using a LOOCV scheme—on these features. At each iteration, a model was trained on every sample except a single test case; the withheld sample was then classified as AD or control by the model. This approach yielded strong predictive metrics, with precision and recall rates of 0.87 and 0.94 for the AD class, and 0.88 and 0.74 for the healthy control class, respectively, along with a predictive score for each sample (score ranging from 0–1), indicating its likelihood of belonging to the AD group.

2.1 SHAP Analysis Pinpoints Personalized Biomarker Sets

To interpret the model's decisions, we used SHAP (Lundberg & Lee, 2017), which computes, for each prediction, a gene-level "importance" score reflecting how much that gene influenced the individual's classification. On average, this analysis identified approximately 175 high-impact genes per patient, representing a personalized biomarker set for each individual sample in the dataset. These gene sets, selected for their high SHAP values (5), provide a detailed view of the unique molecular signatures specific to each patient, distinguishing clearly between healthy and diseased states. Figure 2b illustrates the distribution of SHAP values for several genes across all iterations, highlighting the differential impact of genes on the models' decisions across disease samples.

To ensure reliability, we focused on 720 AD patient samples with predictive scores >0.82 (AD cohort average) for the subsequent analyses. This filtering step excluded borderline samples that might reflect model noise, allowing subsequent biomarker comparisons to center on confidently classified AD cases. Figure 2c presents a t-SNE plot visualizing the distribution of the 720 robustly classified AD cases.

2.2 High-SHAP Genes Converge into Tissue-Specific Biomarker Sets

Using the 720 confidently classified AD patients, we grouped them by their tissue of origin (one of nine brain regions). Within each tissue, each patient had her/his own set of high-SHAP biomarkers. We then intersected the biomarker sets of all AD patients belonging to that tissue, identifying "common" biomarkers—genes deemed critical across all individuals within the same brain region. On average, we found 1 to 36 such genes per tissue, with TCX and PCC showing the greatest overlap, reflecting regionally conserved dysregulation (Fig. 2d). As illustrated in Fig. 2e, the tissue-specific biomarker sets display varying degrees of overlap across different brain regions, with darker cells indicating a greater number of shared genes. These findings confirm that, despite patient-level variability, there are consistently influential genes within specific brain regions, implicating shared mechanisms in AD progression.

2.3 Tissue-specific Biomarkers Demonstrate Clear Biological Significance

To assess whether our Random Forest/SHAP approach identified biologically meaningful genes, we combined all tissue-specific (common) biomarkers—yielding a total of 56 genes across tissues—and performed GSEA via the DAVID Bioinformatics database (14). The enriched pathways and GO terms included membrane-binding functions (e.g., integrin, heme, channel, symporter binding) and extracellular matrix organization (Fig. 2f, g), which are pathways critical for synaptic integrity and disrupted in AD (23). Notably, dysregulated ion transport (Fig. 2h) aligns with Aβ-induced neuronal hyperexcitability (24), confirming that our biomarkers are linked to AD pathophysiology. These findings suggest that our ML pipeline successfully discerns relevant molecular features rather than random signals.

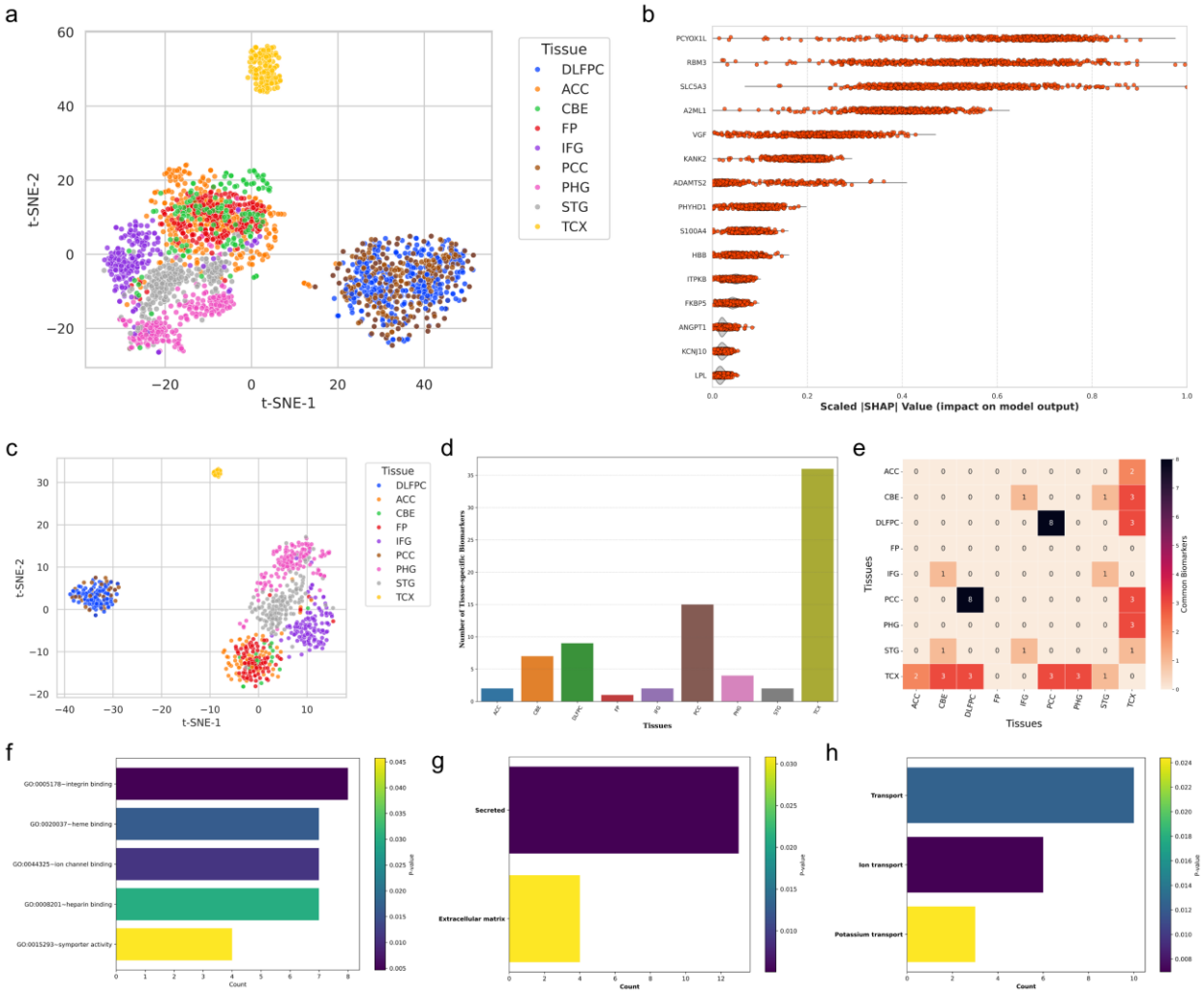

Figure 2. Sample-level and tissue-specific biomarkers reveal regionally conserved molecular dysregulation in Alzheimer's disease.

(a) t-SNE visualization of all 2,105 post-mortem brain samples (AD and controls) colored by tissue of origin, illustrating the overall distribution before filtering.

(b) Scaled SHAP value distributions for representative genes, ranked by their contribution to the Random Forest model's classification of AD vs. control. Each point corresponds to one sample, demonstrating how individual genes differentially influence outputs of the models.

(c) t-SNE projection of the 720 AD samples that exceeded the average predictive score (i.e., "confidently classified" AD cases), showing the final subset used for tissue-specific biomarker analysis.

(d) Bar plot of the number of "common biomarkers" found in each brain region (i.e., high-impact genes shared by all confidently classified AD samples within that tissue). TCX and PCC subtissues exhibit the largest sets.

(e) Heatmap illustrating overlaps of common biomarkers among different tissues; darker cells denote a greater degree of shared genes.

(f–h) GSEA results for the union of all tissue-specific biomarkers (56 genes). (f) Enrichment in membrane-binding activities (integrin, heme, channel, heparin, symporter), (g) shows associations with secreted proteins and extracellular

matrix organization, and (h) emphasizes processes involved in transport, including ion and potassium transport. Collectively, these results underscore the biological relevance of the machine-learning–derived biomarkers, pinpointing pathways central to AD pathogenesis.

3) Subtissue-Specific Biomarkers and Genetic Drivers Reveal Regional Heterogeneity in Alzheimer's Disease

3.1 Four Subtissues per Brain Region Capture Finer Molecular Diversity

Following the identification of patient-level biomarkers, we next sought to characterize molecular heterogeneity at a finer resolution by clustering each brain tissue into four molecularly distinct subtissues. We applied K-means clustering to transcriptomic profiles of samples within each brain tissue, using the union of patient-specific biomarker sets (see previous section) as input features. On the basis of the standard clustering metrics (see *Methods*), we identified four stable clusters per tissue, each containing a number of samples, resulting in 36 total subtissues across nine brain regions. This subdivision captures local molecular variations within a tissue, potentially offering deeper insight into the complex pathological landscape of AD.

3.2 Subtissue-Specific Biomarker Sets Expose Localized AD Mechanisms

Each AD patient carried its own set of high-impact genes (~175 per patient) from the Random Forest–SHAP analysis. To derive subtissue-specific biomarker sets, we intersected the sample-level biomarker lists of all AD samples that fell within the same subtissue cluster. This intersection thus identified genes that were consistently important across individuals in that subtissue. The size of these shared biomarker sets ranged from 4 to 80 genes per subtissue, reflecting variable degrees of molecular commonality (Fig. 3a). Notably, subtissues derived from FP tissue exhibited the fewest overlapping biomarkers (~4), whereas a certain CBE subtissue contained up to 80 shared genes. Such variation underscores the distinct pathobiology within different brain subtissues.

Combining the biomarker sets from all 36 subtissues produced 183 unique genes in total. A complete list of these genes, along with per-subtissue summary statistics, is provided in Table S1. A heatmap of these biomarkers highlights overlapping genes in pairwise subtissue comparisons

(Fig. 3b), revealing that some gene sets are highly region-specific, whereas others span multiple subtissues.

3.3 Functional Enrichment Confirms the Importance of Subtissue Biomarkers

To evaluate the biological significance of these 183 aggregated biomarkers, we performed GSEA. The full per-subtissue breakdown (e.g., the top genes in each subtissue) is available in Table S1. This analysis revealed associations with diverse disease processes, including AD, type 2 diabetes, chronic renal failure, breast cancer, and hypertension (Fig. 3c). These links may reflect shared pathways in metabolic disorders and neurodegeneration—such as insulin signaling deficits and dysregulated apoptosis implicated in AD (25,26)—or broader comorbid mechanisms. As AD emerged among the significantly enriched diseases in the aggregated biomarker set which demonstrates the ability of the Random Forest–SHAP approach to prioritize well-established AD genes and supports the pipeline's overall reliability.

GO terms strongly enriched cell ion transport, differentiation, and angiogenesis, processes that are also recognized as associated with AD (24,27) (Fig. 3d). The analysis also highlighted their involvement in cell secretion and extracellular matrix organization, processes critical in AD advancement (23) (Fig. 3e). Moreover, reactome pathway analysis revealed that biomarkers participate in signal transduction, carbohydrate metabolism, and extracellular matrix organization, further underscoring their comprehensive impact on cellular and molecular functions relevant to AD (23,28) (Fig. 3f).

3.4 Differential Expression Underscores Additional AD-Related Genes

As a complementary approach, we employed Limma (13), to compare AD vs. control expression levels across all tissues, identifying 2,347 ifferentially expressed genes (DEGs) with an absolute log2-fold changes > 0.5 at Bonferroni-adjusted $p < 0.05$ (Fig. 3g). Among the 183 subtissue-specific biomarkers, 88 were significantly upregulated and 72 were downregulated, whereas 23 did not meet the differential-expression threshold yet still presented high SHAP importance. These 23 genes may exert regulatory effects through transcriptional or post-transcriptional mechanisms, as evidenced by several genes enriched in NOTCH1 signaling or reported to have high brain

expression. Taken together, these findings highlight the added value of integrating ML–based feature selection with standard expression-level contrasts to capture a broader spectrum of AD-relevant genes.

3.5 GWAS Data Pinpoint Subtissue-Specific Genetic Drivers

Building on the multifactorial nature of AD and the influential role of genetic variation in disease progression, we next examined genetic drivers in each subtissue via GWAS data matched to our transcriptomic dataset. Specifically, we focused on 96 well-characterized AD-associated genes and their lead variants (12) and compared their mutation rates and allele frequencies in each subtissue against population-wide background allele frequencies in the full patient population (Fig. 3h).

Permutation and chi-square tests pinpointed distinct genetic signatures in each subtissue, underscoring the variability in genetic architecture that may underpin the regional molecular heterogeneity of AD. By integrating these subtissue-specific genetic findings with previously identified transcriptomic biomarkers, we obtained a more comprehensive view of AD pathology at the subtissue level. However, phenotypic outcomes generally arise from the interplay among multiple genes and pathways. Accordingly, to elucidate how genetic drivers interact with transcriptional biomarker pathways, we constructed subtissue-specific gene-gene interaction networks (see *Results Section 4*).

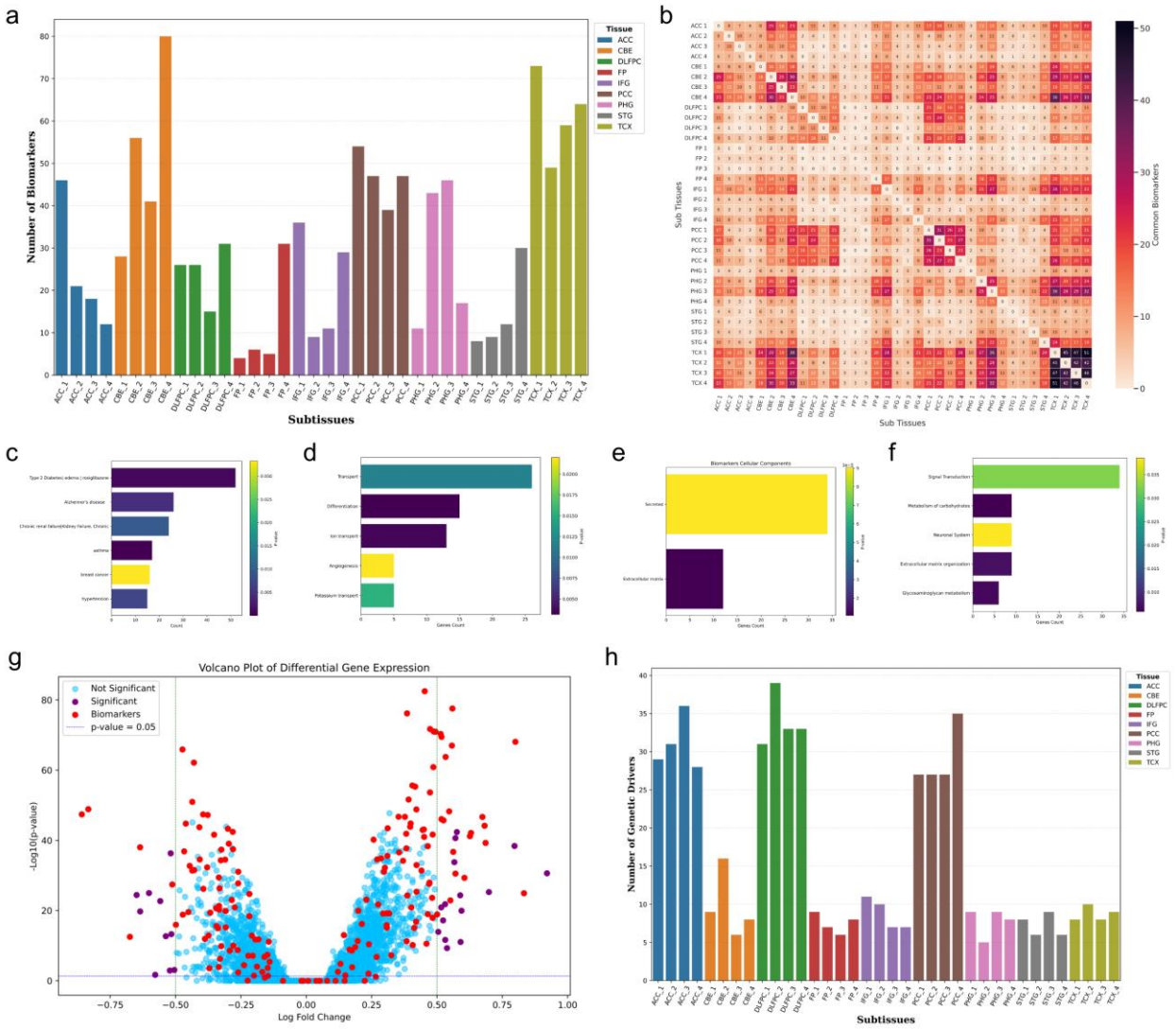

Figure 3. Subtissue-level biomarker discovery, functional enrichment, and genetic driver analysis in AD.

(a) Bar plot of shared biomarkers (y-axis) identified by intersecting patient-level gene sets within each of the 36 subtissues (x-axis), ranging from 4-80 per subtissue/cluster.

(b) Heatmap showing the overlap of biomarker sets across different subtissues. Darker cells depict a higher degree number of shared genes.

(c) Disease enrichment analysis (top six diseases) based on the union of subtissue-specific biomarkers, highlighting comorbid or mechanistically related conditions (e.g., type 2 diabetes, chronic renal failure, and breast cancer).

(d–f) Representative Gene Ontology (GO) and Reactome enrichment results, demonstrating that the aggregated biomarkers are enriched in processes related to cell transport, differentiation, angiogenesis, extracellular matrix organization, and carbohydrate metabolism.

(g) Volcano plot from differential gene expression analysis comparing AD vs. control samples (|log2 fold-change| > 0.5, and Bonferroni-adjusted $p < 0.05$). Biomarkers previously identified by the machine learning approach (colored points) show varied expression patterns, emphasizing the synergy between statistical and ML-driven methods.

(h) Analysis of 96 AD-associated genes in GWAS data, illustrating a bar plot of subtissue-specific genetic drivers. Chi-square and permutation tests detect significant differences in mutation rates compared with background frequencies, underscoring the heterogeneous genetic architecture underlying AD pathophysiology across distinct brain regions.

4) Network Analysis Uncovers Critical Bottleneck Genes as Therapeutic Targets in Alzheimer's Disease

4.1 Subtissue-Specific Gene-Gene Interaction Networks Reveal Key Mediators

To investigate how biomarkers and genetic drivers converge within each brain region, we constructed subtissue-specific gene-gene interaction networks. Each network, derived from RNA-seq profiles of AD samples in a given subtissue, represents a co-expression matrix that highlights potential regulatory relationships among genes. In these matrices, biomarkers (orange nodes) and genetic drivers (green nodes) generally do not interact directly; instead, they are connected through "message-passing" intermediates (blue nodes) that mediate signaling cascades influencing AD progression and ultimately affecting the phenotype. A representative example from one neocortex subtissue is shown in Figures 4a–4c. Figure 4a displays the entire subtissue co-expression network, whereas Figure 4b isolates only biomarkers, genetic drivers, and their intermediate connections. Figure 4c further highlights high-centrality (hub) genes in red. Figure 4d shows the variability in number of message-passing intermediate genes among subtissues.

4.2 Prioritizing Critical Bottleneck Genes through Centrality Metrics

In each filtered subtissue-specific gene-gene interaction network which included only biomarkers, genetic drivers, and the intermediate message-passing genes, we ranked the constituent genes by multiple centrality metrics (e.g., betweenness, and closeness). These metrics assess a gene's connectivity and influence within the network, pinpointing those with the most significant roles in mediating cellular communication within the subtissue network. Genes consistently scoring high in connectivity and low in clustering were designated as candidate hub genes, as they appear pivotal in bridging communication between biomarkers and genetic drivers within the filtered network. This initial analysis yielded 22–30 candidate hub genes per subtissue.

To prioritize underexplored therapeutic possibilities, we then filtered out well-characterized AD genes from each hub-gene list, focusing on less-studied but highly ranked genes. These critical bottleneck genes likely offer novel insights into AD pathophysiology and could serve as new therapeutic targets. The number of critical bottleneck genes varied across subtissues (Fig. 4e), reflecting the heterogeneous genetic architecture of AD in different brain regions. A complete listing of these bottleneck genes—including subtissue affiliations, and annotation details—can be found in Table S1.

Ultimately, unifying the critical bottleneck genes from all subtissues yielded 262 unique drug target candidates. Figure 4f illustrates how these bottlenecks interact in the broader human proteome (16). By integrating biomarkers, genetic drivers, and their bottleneck genes, this set underscores a systems-level perspective on AD pathology and suggests new directions for drug discovery and therapeutic interventions.

4.3 Functional Enrichment Links Bottleneck Genes to Core AD Pathobiology

To evaluate the biological relevance of the 262 consolidated bottleneck genes, we performed GO and Reactome enrichment analyses (Figs. 4g–4j). The majority of these genes encode membrane or synaptic junction proteins involved in ion transport, adhesion, and differentiation—key processes linked to AD pathology (24,29). Other enriched functions included extracellular matrix organization and cellular secretion, both of which have been implicated in AD progression (23,30).

Reactome analysis highlighted processes such as signal transduction, nervous system development, small-molecule transport, actin cytoskeleton regulation, and axon guidance—all relevant to the molecular mechanisms of AD (24,30,31). Notably, cytoskeletal dysregulation has gained attention for its role in synaptic integrity (31), indicating that it as a potential area of further investigation.

Moreover, many of these bottleneck genes are associated with additional diseases—ranging from diabetes to neuropsychiatric disorders—suggesting shared mechanisms and underlining broader implications for comorbidities in AD. Together, these findings suggest that the identified

bottleneck genes warrant deeper exploration as candidate targets for pharmacological intervention, which we address in the subsequent section on drug repurposing.

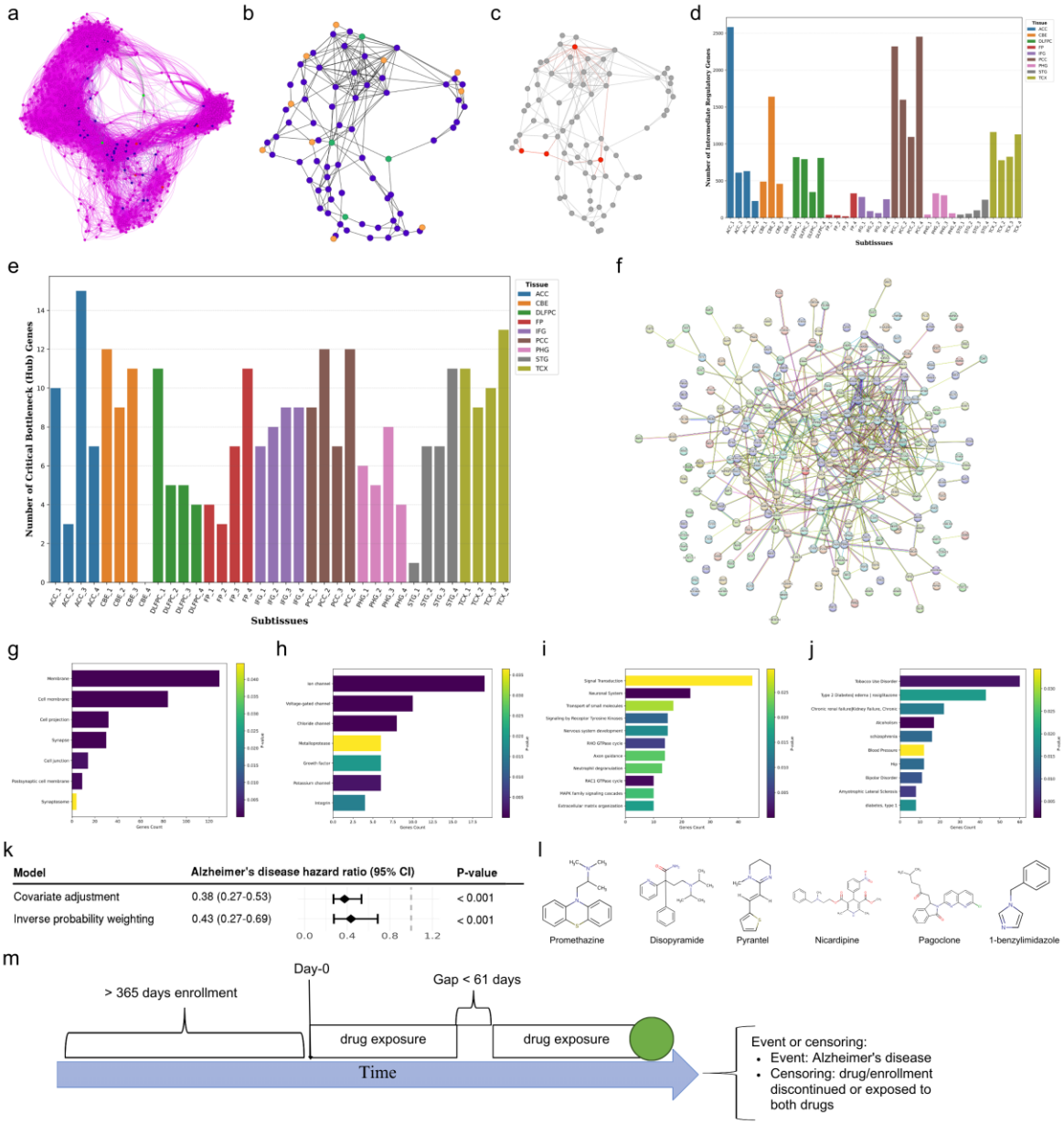

Figure 4. Subtissue-specific gene-gene interaction networks, identification of critical bottleneck genes, and their functional relevance in AD.

(a) Weighted gene co-expression network (magenta) from a representative neocortex subtissue, capturing all genes expressed in that cluster.

(b) The same network filtered to include only biomarkers (orange nodes), genetic drivers (green nodes), and intermediate "message-passing" genes (blue nodes).

(c) Highlighting hub genes (red nodes) identified by multiple centrality measures (e.g., degree, betweenness, PageRank).

(d) Bar chart showing the number of intermediate bridging genes for each of the 36 subtissues; one was excluded for insufficient samples.

(e) Variations in the counts of critical bottleneck genes (i.e., highly ranked novel hub genes) across subtissues, reflecting regional heterogeneity.

(f) STRING-based protein–protein interaction map of the final 262 bottleneck genes, illustrating their interconnectivity in the broader human proteome.

(g–j) Functional enrichment analyses of these bottleneck genes, including cellular component (g), molecular function (h), Reactome pathway (i), and disease associations (j). The enriched terms highlighted roles in membrane localization, synapse organization, ion channel activity, signal transduction, cytoskeletal regulation, and various comorbid conditions such as type 2 diabetes.

(k) Pharmacoepidemiologic analysis of the associations of promethazine versus cyproheptadine with AD (forest plot) demonstrating a hazard ratio under different adjustment methods, supporting the therapeutic relevance of one identified drug candidate in real-world patient data.

(l) molecular structures of the six repurposed candidate drugs

(m) Illustration of real-world pharmacoepidemiologic study design.

5) Drug Repurposing Suggests Multi-Targeted Strategies for AD Treatment

5.1 Knowledge-Graph Analysis Discovers FDA-Approved Drugs Targeting Bottleneck Genes

To identify multi-target drug candidates against our 262 bottleneck genes, we leveraged the Bioteque knowledge graph (18). This resource harmonizes over 150 data sources into a unified network of more than 450,000 biological entities (such as 20108 genes and 137396 compounds) and 30 million relationships—encompassing drug–gene, gene–disease, and other cross-domain interactions. By using the Bioteque's precomputed embeddings and traversing multi-step metapaths (e.g., compound–gene–gene), we systematically evaluated drug–gene affinity with cosine similarity and confirmed strong predictive performance (Area Under the Curve (AUC)-based reconstruction) at a 0.65 similarity cutoff. These precomputed embeddings not only reduce dimensional complexity but also preserve topological signals in the original network, enabling efficient retrieval of drug–gene associations.

In line with the Bioteque's demonstration that multi-step 'metapaths' (e.g., compound-interacts-gene-coexpresses-gene) can uncover novel therapeutic relationships, our analysis traverses compound–gene routes to pinpoint drugs with plausible multi-target activities relevant to AD. Specifically, we focused on four embedding "routes" (metapaths) that connect compounds to genes through different intermediate relationships ("interacts" or "coexpresses", "codepends", and "protein-protein interacts"), quantifying gene–drug affinity with cosine similarity. These metapaths capture distinct biological mechanisms, from direct binding to indirect regulatory effects, ensuring a holistic view of drug-target relationships.

For each metapath, we first compared each of the 262 bottleneck genes (identified via network analysis) to every compound in the Bioteque, retaining the top five hits per gene based on the similarity/confidence score. By merging these hits across the four metapaths, we identified a total of 2355 high-confidence drug–gene pairs spanning 225 bottleneck genes and 1600 unique compounds. We then applied two filtering criteria—(i) a cosine similarity of 0.65 or higher, and (ii) targeting of at least two bottleneck genes—yielding six FDA-approved drugs (Fig 4l): pyrantel (5 targets), promethazine (3 targets), disopyramide (3 targets), nicardipine (2 targets), 1-benzylimidazole (2 targets), and pagoclone (2 targets).

Three of these candidates (disopyramide, nicardipine, and 1-benzylimidazole) are predominantly cardiovascular agents that address conditions such as arrhythmias or hypertension. Moreover, pyrantel and promethazine exhibit anti-inflammatory or neuromodulatory properties, suggesting particular relevance for AD interventions. pagoclone, an anxiolytic partial Gamma-Aminobutyric Acid (GABA)-A receptor agonist, presents a novel therapeutic avenue without the sedative drawbacks of related compounds. The following subsections describe each agent's pharmacologic attributes and their potential impact on AD.

5.2. Predicted Repurposed Drugs Show Diverse but Similar Pharmacological Profiles

Our analyses highlighted six FDA-approved drugs (Fig 4l) —promethazine, disopyramide, pyrantel, nicardipine, pagoclone, and 1-benzylimidazole—that, despite disparate primary indications, converge on mechanisms potentially relevant to AD. Below, we summarize their documented pharmacological actions and AD-related rationales.

promethazine (Phenergan) is a first-generation H1-antihistamine and an antagonist of the D2 dopamine receptor with strong sedative effects and moderate anticholinergic properties, used for several allergic reactions (32). It also exhibits N-Methyl-D-Aspartate (NMDA) receptor antagonism, potentially conferring neuroprotective benefits by reducing excitotoxic damage. Clinically, promethazine is widely used for allergic symptoms, nausea, and adjunctive management of psychosis-induced aggression (33). *In vitro*, promethazine scavenges reactive oxygen species and modulates genes such as COX-2, suggesting anti-neuroinflammatory properties (34). A screening has shown that promethazine can bind amyloid-β plaques in post-mortem tissue, raising possibilities for modifying or imaging amyloid pathology (35). Additionally, when it is used alongside haloperidol for rapid tranquilization, it may also alleviate agitation or aggression in AD patients (33).

Disopyramide (Norpace), a class Ia antiarrhythmic agent, is employed to manage ventricular tachycardia and hypertrophic cardiomyopathy, reducing myocardial contractility and potentially benefiting neurological conditions through the modulation of voltage-gated sodium channels (36). While early AD is often accompanied by aberrant network hyperactivity or subclinical seizures, a sodium-channel blocker could hypothetically stabilize firing rates and prevent excitotoxic damage (37).

Pyrantel, which is used to treat several worm infections, is a depolarizing neuromuscular blocker that mimics acetylcholine at nicotinic receptors in parasitic nematodes. It is FDA-approved for treating pinworm and hookworm infections (38). By activating nicotinic acetylcholine receptors, pyrantel can bolster synaptic plasticity and dampen neuroinflammation, aligning with cholinomimetic strategies in AD (39). Additionally, similar nicotinic receptor agonists (e.g., varenicline) have shown cognitive or anti-inflammatory benefits in models, reducing AD pathology (Mitra et al., 2020).

nicardipine (Cardene IV), an FDA-approved drug used to treat high blood pressure, is a dihydropyridine calcium-channel blocker that reduces Ca^{2+} influx in vascular smooth muscle, improves cerebral perfusion and lowers blood pressure (40). By preventing Ca^{2+} overload and boosting cerebral blood flow, nicardipine may protect neurons from ischemic and inflammatory

damage (41). Epidemiological data suggest that dihydropyridines (nifedipine, nilvadipine) slow cognitive decline via antiamyloid or vasoprotective mechanisms (42). nicardipine is used for acute stroke management, implying potential synergy in AD, where chronic hypoperfusion accelerates pathology (Duncombe et al., 2017).

pagoclone is a non-benzodiazepine partial GABA-A receptor agonist designed for anxiety and tested for stuttering. Its partial agonism reduces anxiety with less sedation or dependence than full benzodiazepines (44). Mild GABA enhancement can quell neuronal hyperexcitability, which is frequently observed in early AD, without the cognition-impairing effects of benzodiazepines (45). Moreover, the anxiolytic profile of pagoclone may help manage agitation or anxiety in AD patients (45).

1-benzylimidazole, which is recognized for its positive inotropy and thromboxane A_2 synthase inhibition, has been explored as a cardiotonic and anti-inflammatory agent (46). Thromboxane A_2 is not only a platelet aggregator but also a pro-inflammatory mediator that can be produced in the brain. By inhibiting Thromboxane A_2 production, 1-benzylimidazole may enhance cerebral perfusion and reduce pro-inflammatory eicosanoids, addressing microvascular deficits in AD patients (47).

Although each candidate poses distinct caveats—anticholinergic risks (disopyramide, promethazine) or uncertain Central Nervous System (CNS) penetration (pyrantel)—they share mechanisms potentially relevant to multiple AD pathways. promethazine and pagoclone may mitigate neuropsychiatric symptoms and excitotoxicity, nicardipine and 1-benzylimidazole target vascular and inflammatory processes, and pyrantel can bolster nicotinic cholinergic function. However, the potent antimuscarinic profile of disopyramide demands caution. Overall, these findings underscore the value of multi-target drug screening in AD and call for further research to determine whether such repurposed agents can meaningfully alter disease trajectories or symptom burden.

5.3. Drug–Entity Network Suggests Convergent Pathways with Potential AD Relevance

To expand on each compound's potential mechanisms, we extracted node embeddings from the Bioteque knowledge graph (18) and computed cosine similarities between each repurposed drug and the nodes of two entities, namely molecular functions and pathways. Retaining the top five hits per compound allowed us to pinpoint commonly repeated features that might underlie shared pharmacological effects.

Several compounds clustered around metabolic or contractile pathways—such as glycogen breakdown (glycogenolysis) and striated muscle contraction— have long been viewed as muscle-specific processes but are now recognized in AD due to astrocyte-regulated glycogen metabolism affecting neuronal signaling (48), and muscle-derived factors influencing hippocampal network development (49). We also identified repeated hits for processes such as DNA methylation and calcium-dependent regulation, which are known contributors to neuroinflammation and synaptic dysfunction in AD (50,51).

Next, we identified repeated occurrences of myosin binding, calcium-dependent kinase regulation, and RNA polymerase II transcription factor binding among the top similar molecular functions. Although these are not classically "Alzheimer's-specific" terms, dysregulation of calcium signaling and altered gene transcription are integral to AD pathophysiology (51). Hence, the network-level findings suggest multi-target potential of our candidate drugs. Recognizing these convergent pathways sets the stage for further validation: in the next section, we examine whether one of these candidates (promethazine) indeed demonstrates real-world benefits against AD in large-scale Electronic Health Records (EHR) data.

6. Promethazine is Associated with a Reduced AD Risk in Real-world Data

We identified 353856 individuals with promethazine exposure and 10877 individuals with cyproheptadine, a H1-antihistamine drug similar to promethazine (19), exposure. Figure 4m depicts the study design. The demographics of the study population are presented in Table S2. Compared with cyproheptadine exposure, promethazine exposure was associated with a reduced risk of AD in covariate-adjusted Cox model (HR (Hazard Ratio) =0.38, 95% CI: 0.27-0.53, and p <0.001, Fig. 4k) and Cox model using inverse probability of treatment weighting (HR =0.43, and P <0.001, Fig. 4k). The full results of the covariate-adjusted Cox model are presented in Table S3.

This significant association between promethazine exposure and a reduced risk of AD, as evidenced by our robust covariate-adjusted Cox model, suggests potential neuroprotective properties that warrant further investigation. These findings could inform future clinical trials and healthcare strategies aimed at integrating promethazine into broader AD management protocols.

Methods

1) Data Collection and Preprocessing

We integrated bulk RNA-SEQsequencing and Genome-Wide Association Study (GWAS) data, from three independent large-scale AD brain tissue studies: the Religious Orders Study and Rush Memory and Aging Project (ROSMAP) (6), the Mount Sinai Brain Bank study (MSBB) (7), and the Mayo RNA-seq study (MAYO) (8), which were obtained via the Accelerating Medicines Partnership - AD (AMP-AD) Knowledge Portal (https://www.synapse.org/Synapse:syn21241740 and https://www.synapse.org/Synapse:syn22264775) (9). In total, our curated dataset comprised 2105 post-mortem brain tissue samples (1363 AD and 742 control) from 835 unique individuals (528 females and 307 males) collected from nine distinct brain tissues: Anterior Cingulate Cortex (ACC), Cerebellum (CBE), Dorsolateral Prefrontal Cortex (DLFPC), Frontal Pole (FP), Inferior Frontal Gyrus (IFG), Posterior Cingulate Cortex (PCC), Parahippocampal Gyrus (PHG), Superior Temporal Gyrus (STG), and Temporal Cortex (TCX). Table 1 summarizes the distribution of samples and subjects across the nine brain regions.

As our analysis emphasized subtissue-level biomarkers and genetic drivers, and because samples were inherently separated by tissue source, we opted not to perform a formal batch correction during our harmonization. Although batch correction can be crucial when the same tissues or platforms overlap across cohorts, our evaluation revealed that the expression profiles largely reflected underlying tissue differences rather than technical biases. Correcting for “batches” in this situation would risk conflating genuine subtissue signals with artificial adjustments. Therefore, our final pipeline uses the direct gene expression and genomic data from each cohort, only regressing out only clinical covariates (apart from diagnosis) to minimize confounding. All subsequent analyses were performed on this harmonized dataset.

Table 1. Overall Cohort Description: Demographics, Brain Tissue Distribution, and Sample Characteristics

Tissue Name	Cohort	Total Samples	AD Samples	Control Samples	Male Samples	Female Samples	Total Subjects
ACC	ROSMAP	265	171	94	90	175	265
DLFPC	ROSMAP	436	293	143	143	293	429

PCC	ROSMAP	250	151	99	97	153	249
FP	MSBB	215	146	69	83	132	197
IFG	MSBB	201	132	69	86	115	181
PHG	MSBB	226	155	71	84	142	168
STG	MSBB	220	156	64	93	127	181
CBE	MAYO	144	79	65	69	75	144
TCX	MAYO	148	80	68	66	82	148
ALL TISSUES	TOTAL	2105	1363	742	811	1294	1962

Table 1. This table summarizes the distribution of samples and unique individuals across multiple brain tissues and studies, including the number of Alzheimer's disease (AD) vs. control samples, the breakdown by sex, and total individuals per cohort.

2) Machine Learning Classification and Model Interpretation

To identify patient-specific biomarkers, we implemented a Random Forest classifier using scikit-learn (v1.4.0) (10) in Python (v3.10.6). A set of 5,000 highly variable genes was selected as input features for the models. Notably, a number of well-characterized AD genes (e.g., APOE) were automatically excluded due to minimal expression changes among samples. We employed a LOOCV strategy, ensuring that each sample was independently withheld from training. Our model was optimized through 10-fold stratified cross-validation via a grid search, and the optimal parameters were determined to be {n_estimators=722, max_depth=38, min_samples_split=5, min_samples_leaf=4, max_features=0.11}, which achieved an F1 score of 0.88, precision of 0.84, recall of 0.93, and Receiver Operating Characteristic Area Under the Curve (ROCAUC)of 0.90.

To elucidate gene-level contributions to model predictions, we applied the TreeExplainer from the SHAP framework (11). The classification predictive score for each sample was assessed via the model's *predict_proba()* function. For each sample, SHAP values were computed, identifying on average 175 high-impact genes that served as personalized biomarkers distinguishing AD samples from control samples.

3) Subtissue Identification and Subtissue-Specific Biomarkers and Genetic Drivers

3.1 K-Means Clustering

We next sought to detect finer-scale molecular variation within each of the nine brain tissues. For each tissue, we assembled a matrix containing only samples from that tissue (both AD patients and

controls). The feature set comprised the union of all patient-level biomarkers associated with that tissue's AD samples, i.e., genes with high SHAP values in at least one AD sample from that region.

Using this tissue-restricted feature matrix, we performed K-means clustering (k=4) to segment each tissue into four "subtissues." The number of clusters was chosen on the basis of elbow-method plots (assessing total within-cluster sum of squares) and silhouette scores. This process yielded 36 total subtissues (4 per tissue × 9 tissues).

3.2 Subtissue-specific Biomarkers Definition

We intersected the patient-level biomarker lists of all AD samples within each of these subtissue clusters to define 'subtissue-specific biomarker sets' (ranging from 4 to 80 genes per cluster). Details of these gene sets and their associated statistics are available in Table S1. Specifically, (1) each cluster (subtissue) contained a subset of AD samples, each with its own ~175 patient-level biomarkers, and (2) we took the intersection (common genes) across these AD samples. Genes appearing in all AD samples of that subtissue were designated "subtissue-specific biomarkers." This approach ensures that the resulting genes are consistently highly impacted in the same cluster of AD samples, highlighting regionally shared dysregulations. Subtissue-specific biomarker set sizes ranged from 4 to 80 genes, reflecting heterogeneity among subtissues.

3.3 Identifying Subtissue-Specific Genetic Drivers

We curated a list of 96 well-characterized AD-associated genes (and their lead single nucleotide polymorphisms (SNPs)) from recent GWAS meta-analyses (Andrade-Guerrero et al., 2023). For each sample in our study, per-allele genotype data for these SNPs were extracted from the matched GWAS files.

To pinpoint region-specific genetic drivers, we computed each SNP's mutation rate and allele frequency within every subtissue (AD samples only) and then performed the following: (1) we compared each subtissue's rates (e.g., minor allele frequency) against the full AD cohort as a background, (2) chi-square tests, followed by empirical permutations, assessed whether a given SNP's enrichment in a subtissue was greater than expected by chance, (3) we assigned SNP-associated genes to a subtissue if their SNP(s) exhibited significant enrichment ($p < 0.05$ after multiple-testing correction). These genes, together with the subtissue-specific biomarkers, were subsequently used to construct gene-gene interaction networks.

4) Statistical Analysis and Gene Set Enrichment

Differential gene expression was assessed via the Limma package (v3.62) in R (13). Genes with an absolute log2 fold change > 0.5 and a Bonferroni-adjusted p value < 0.05 were considered significantly different between the AD samples and control groups.

Gene set enrichment analysis (GSEA) was performed via the DAVID database (14) to evaluate the biological functions of tissue- and subtissue-specific biomarkers. Enriched Gene Ontology (GO) terms and Reactome pathways highlighted processes such as membrane binding, extracellular matrix organization, and ion transport—pathways that are critically involved in AD pathogenesis.

5) Gene-Gene Interaction Network Construction and Critical Bottleneck Genes

We employed Weighted Gene Co-expression Network Analysis (WGCNA) (15) to construct subtissue-specific gene-gene interaction networks. For each subtissue (as defined by K-means clustering), we assembled three categories of genes: (1) Subtissue-specific biomarkers (i.e., the genes consistently identified by SHAP across all AD samples in that cluster), (2) genetic drivers (from the 96 AD-associated GWAS genes were found to be significantly enriched in that subtissue), and (3) all other genes whose expression levels correlated with either biomarkers or genetic drivers in that subtissue. The combined gene set ensured that both disease-relevant signatures (biomarkers/drivers) and potential intermediates were captured. To preserve biologically realistic network sizes, we retained the top edges until the final network had an edge density of ~0.5%, aligning with typical protein–protein interaction densities in the human proteome (16). Visualization of networks was facilitated via String database (16) and Gephi (17).

Although we included “all other genes” in the adjacency matrix, our focus was on how biomarkers and genetic drivers interconnect. For each subtissue network, we traced the shortest paths between biomarkers and drivers, flagging any nodes on these paths as potential “message-passing” intermediates.

We computed multiple centrality measures (e.g., betweenness centrality, PageRank, closeness, and eigenvector centrality) to quantify each gene’s importance in relaying network information. Genes consistently scoring in the top ranks across multiple metrics were designated as high-centrality “hub” genes, reflecting their importance in bridging multiple AD-relevant pathways. This step yielded 22–30 candidate hub genes per subtissue. We then focused on the hub genes ranked higher than the extensively characterized AD genes (e.g., APOE) to explore novel candidates, yielding 1-

15 “bottleneck” genes per subtissue (Fig. 4e). Combining bottleneck gene lists across all 36 subtissues produced a nonredundant set of 262 candidate targets.

6) Drug Target Identification and Repurposing Drugs

Drug repurposing analysis was conducted via the Bioteque knowledge graph (Fernández-Torras et al., 2022), which integrates 30 million relationships across 12 biomedical entity types. We systematically queried four metapaths to model compound-gene interactions: (1) CPD-int-GEN: sirect pharmacological interactions (e.g., binding, inhibition), (2) CPD-int-GEN-cdp-GEN: compound effects mediated by codependent genes, (3) CPD-int-GEN-cex-GEN: compound-gene associations via co-expressed intermediaries, (4) CPD-int-GEN-ppi-GEN: compound effects propagated through protein interactors.

We focused solely on 262 bottleneck genes identified from our subtissue-specific interaction networks (see *Results*). For each metapath, node embeddings (128-dimensional vectors) were extracted, and cosine similarities between all 262 bottleneck genes and 137396 compounds were computed. We then retained only the top five compounds per gene (i.e., those with the highest similarity), thereby discarding low-confidence pairs and reducing noise.

We concatenated the reduced results from each route, resulting in a final dataframe of 2355 gene–drug pairs covering 225 bottleneck genes and 1600 unique drug entities. We then plotted the distribution of cosine similarities across these pairs to select a threshold of 0.65. Next, we filtered out drugs interacting with only a single bottleneck gene, as our aim was to highlight multi-target therapeutic leads. From this process, six Food and Drug Administration (FDA)-approved drugs were found to surpass both criteria—Disopyramide, nicardipine, 1-benzylimidazole, pagoclone, promethazine, and pyrantel.

7) EHR Validation Study

We used Optum’s de-identified Clinformatics Data Mart Database (Clinformatics, years: 2007-2021). Clinformatics is derived from a database of administrative health claims for members of large commercial and Medicare Advantage health plans. The Indiana University Institutional Review Board (IRB) designated this study as exempt.

We used active comparator design by selecting cyproheptadine (10877 individuals) as the comparator for promethazine (353856 individuals), as both drugs are tricyclics and first generation H1-antihistamines (19). Figure 4m illustrates the study design. We defined the initiation date (e.g.,

day-0) as the first date of exposure. We included individuals who started on promethazine and/or cyproheptadine, were aged ≥60 years and had an enrollment period of ≥2 years. We excluded individuals that had both drugs exposure on day-0, only 1-day of exposure, and missing gender information; as well as individuals with the following conditions prior to day-0: <365 days of enrollment, AD, dementia, AIDS, solid tumors without metastasis, lymphoma, and/or metastatic cancer.

We used International Classification of Diseases (ICD) codes (e.g., ICD-9 3310, ICD-10 F00*, and ICD-10 G30*) to define AD (20,21). We defined the outcome as the time from day-0 to the first AD diagnosis date. We defined the censoring date as the earliest of discontinuation of exposure (e.g., the last date of exposure without exposure in the next 60 days), concurrent exposure to both drugs, or discontinuation from enrollment.

We collected covariates on demographics including age, gender, race and index year of day-0. Demographics of the study population are provided in Table S2. Additionally, we used the R package Comorbidity to define alcohol use disorder, blood loss anemia, cardiac arrhythmias, congestive heart failure, coagulopathy, chronic pulmonary disease, deficiency anemia, depression, diabetes status (uncomplicated and complicated), drug abuse, fluid and electrolyte disorders, hypertension status (uncomplicated and complicated), hypothyroidism, liver disease, obesity, other neurological disorders, paralysis, pulmonary circulation disorders, psychoses, peptic ulcer disease excluding bleeding, pulmonary circulation disorders, peripheral vascular disorders, renal failure, rheumatoid arthritis or collaged vascular disease, valvular disease, and weight loss. Moreover, we identified fall, hearing impairment/loss and vision impairment according to Cheng et al. (22).

We used Cox models to estimate hazard ratios (HRs), 95% confidence intervals (CIs), and *p* values. First, we fitted a covariate-adjusted Cox model by adjusting all covariates. Second, we conducted a sensitivity analysis utilizing inverse probability of treatment weighting with the propensity score. We used logistic regression model to estimate the propensity score by controlling for all covariates. The Cox model included the exposure status of promethazine/cyproheptadine and used inverse probabilities of treatment as weights. Covariate-adjusted Cox model results are presented in Table S3. All pharmacoepidemiologic analyses were conducted in R.

Discussion

In this study, we introduce PRISM-ML (PRecision-medicine using Interpretable Systems and Multiomics with Machine Learning), a framework which integrates interpretable ML with multiomics data to dissect the molecular complexity of AD (Fig. 1). By simultaneously analyzing

transcriptomic and genomic profiles from the same patient cohort, we uncovered patient-level biomarkers that reveal notable heterogeneity within and across brain regions. Notably, by clustering patient samples we identified 36 "subtissues" spanning nine brain areas, emphasizing localized molecular diversity that underpins AD pathogenesis.

Building on these findings, we constructed subtissue-specific gene-gene interaction networks to clarify how biomarkers and genetic variants converge on shared pathways. Within these networks, 262 high-centrality "bottleneck" genes emerged as potential drivers of AD progression. Leveraging a knowledge-graph approach, we then pinpointed six FDA-approved drugs with putative multi-target effects, suggesting a promising avenue for therapeutics that address multiple disease pathways in concert.

Despite these advances, some limitations warrant consideration. First, our analysis focused on transcriptomic and genomic data; thus, we have yet to incorporate proteomic, epigenetic, or metabolomic factors that may also shape AD progression. Second, one subtissue cluster had too few samples for reliable network construction, potentially excluding unique molecular features. Third, our use of bulk RNA-seq provides a broad overview but cannot resolve the contributions of individual cell types within each region, which are crucial in AD pathogenesis (52), an area ripe for exploration via single-cell or spatial transcriptomic methods. Nonetheless, we addressed tissue heterogeneity through our LOOCV strategy which led to patient-level biomarker identification.

Finally, our drug repurposing discoveries rely on association-based knowledge graph embeddings, which do not specify whether the predicted interactions are agonistic or antagonistic. Further biochemical and clinical studies are needed to validate these targets and elucidate their modes of action. However, our pharmacoepidemiologic findings on promethazine's protective association underscore the potential power of combining systems-level analyses with real-world evidence to accelerate the discovery of multi-target therapies for AD.

Our research has several strengths that underscore its significance in AD research. First, by leveraging SHAP (5), values, we have addressed the interpretability gap often associated with ML models, clearly illustrating each gene's contribution to classification of each AD sample. Second, our focus on subtissue-specific changes rather than broad tissue-level analyses enabled a more precise dissection of the regional heterogeneity of AD. Third, integrating transcriptomic and genomic data from the same cohorts provided a unified view of how genetic risk factors converge with altered gene expression, thereby improving the construction of networks that capture the systemic complexity of AD. Fourth, by adopting a LOOCV strategy, our study ensures that the findings are robust and personalized, addressing patient-specific disease manifestations and contributing to precision medicine. Finally, we prioritized and characterized novel bottleneck

genes, rather than reiterating the well-studied AD genes, revealing underexplored therapeutic avenues.

In parallel, our GSEA pinpointed dysregulated pathways—particularly those linked to synaptic function, signal transduction, cellular transport, and the actin cytoskeleton (Pelucchi et al., 2020)—that are not typically emphasized in AD research. By confirming their enrichment across subtissue-level biomarkers as well as bottleneck genes, we highlight underappreciated molecular processes that may offer novel therapeutic avenues.

In addition to pinpointing new targets, our analysis predicted six FDA-approved drugs (Fig. 4l) with strong multi-target potential based on their interactions with critical bottleneck genes. Three of these—Disopyramide, nicardipine, and 1-benzylimidazole—are used primarily for cardiovascular conditions, whereas promethazine, pagoclone, and pyrantel modulate neuronal or neuromuscular pathways. Although each agent poses distinct side-effect concerns—particularly anticholinergic load in older adults—this cross-pathway coverage underscores the promise of multi-target strategies for complex disorders such as AD. Mechanistic overlaps suggest that promethazine and pagoclone may alleviate neuropsychiatric symptoms and excitotoxicity, nicardipine and 1-benzylimidazole could address vascular and inflammatory dysregulation, and pyrantel might bolster cholinergic function; however, the antimuscarinic properties of disopyramide warrant caution. Taken together, these findings highlight the need for further *in vivo* and clinical validation to determine whether these repurposed candidates can meaningfully alter disease progression and improve patient outcomes.

The real-world evidence from our pharmacoepidemiologic study utilizing Optum's Clinformatics Data Mart Database (2007-2021) provides compelling support for the protective effect of promethazine against AD. Using an active comparator design with cyproheptadine, another first-generation H1-antihistamine (Kalpaklioglu & Baccioglu, 2012), our analysis of over 364000 individuals (demographic details in Table S2) demonstrated that promethazine exposure was associated with a significantly reduced risk of AD (HR = 0.38, 95% CI: 0.27-0.53) (full Cox model results in Table S3). This finding was further validated through sensitivity analysis via inverse probability of treatment weighting (HR = 0.43). While these results are promising, they should be interpreted within the context of certain limitations, including potential unmeasured confounding effects, possible misclassification in health insurance records, and limited generalizability to populations outside commercial or Medicare Supplemental health insurance plans. Notably, healthcare claims data are vulnerable to misclassification of mild or early AD, which can bias hazard ratios. Moreover, a study (32) has shown that a high anticholinergic load can worsen confusion causing delirium in older adults; therefore, chronic use of promethazine in AD patients demands careful risk–benefit assessment. Future studies should validate these results in broader, more diverse cohorts and incorporate rigorous causal-inference methods to address residual confounding.

Moving forward, our findings set the stage for deeper investigation into these identified candidates and their biological interactions. Rigorous *in vitro* and *in vivo* assays can clarify whether each agent's mechanisms—agonistic or antagonistic—truly counter AD pathologies. In parallel, novel computational methods, including neural networks and transformer-based models with interpretability tools (53), could refine biomarker discovery, whereas expanded omics data layers (e.g., proteomics, metabolomics, and epigenetics) might yield a fuller picture of the molecular architecture of AD. Future investigations should incorporate single-cell and spatial transcriptomics, which can resolve the cell-type-specific disruptions masked by bulk RNA profiling. By isolating distinct neuronal and glial populations within discrete brain regions, these advanced approaches could deepen our understanding of how localized molecular changes shape AD pathology, ultimately guiding more precise diagnostic markers and therapeutic interventions.

Ultimately, we envision PRISM-ML serving as a robust bridge between foundational multi-omics research and clinical application, aiming to unite basic discovery with patient-centered outcomes. By coupling interpretable ML, targeted biomarker discovery, and real-world evidence, our framework paves the way for multi-pathway therapeutics that can be customized to individual molecular profiles. Future studies incorporating proteomics and single-cell spatial data could further resolve AD's molecular complexity, while leveraging open resources like the AMP-AD Knowledge Portal (9) will enhance collaborative precision medicine.

Conclusion

In this work, we developed PRISM-ML (PRecision-medicine using Interpretable Systems and Multiomics with Machine Learning), an interpretable ML framework integrated with multiomics data (bulk RNA-seq and genomics) to illuminate key molecular mechanisms underlying AD. By identifying patient-level biomarkers and constructing subtissue-specific gene-gene interaction networks, we revealed critical bottleneck genes and highlighted new paths for therapeutic intervention. Our data-driven knowledge graph-based approach led to the discovery of six repurposable drugs that target multiple AD-relevant pathways simultaneously, marking a shift from conventional single-target strategies. Real-world evidence, including pharmacoepidemiologic validation of promethazine, underscores the clinical promise of our findings, although further experimental and clinical studies are needed to refine the mechanistic details and therapeutic efficacy.

As precision medicine gains momentum, our integrated pipeline—combining molecular signatures, knowledge graph-based repurposing, and real-world data validation—offers a powerful template for unraveling heterogeneity of complex diseases and accelerating the development of

targeted, multi-pathway drug treatments. While further experimental work is necessary to validate our findings, this study paves the way for transformative advancements in AD treatment and beyond, potentially accelerating the shift toward more personalized medicine in clinical practice.

List of abbreviations

- AD: Alzheimer's Disease
- PRISM-ML: PRecision-medicine using Interpretable Systems and Multiomics with Machine Learning
- GWAS: Genome-Wide Association Study
- LOOCV: Leave-One-Patient-Out Cross-Validation
- SHAP: SHapley Additive exPlanations
- WGCNA: Weighted Gene Co-expression Network Analysis
- DEGs: Differentially Expressed Genes
- t-SNE: t-Distributed Stochastic Neighbor Embedding
- GO: Gene Ontology
- GSEA: Gene Set Enrichment Analysis
- HRs: Hazard Ratios
- EHR: Electronic Health Records
- CNS: Central Nervous System
- RNA-seq: RNA Sequencing
- SNPs: Single Nucleotide Polymorphisms
- ICD: International Classification of Diseases
- AMP-AD: Accelerating Medicines Partnership - Alzheimer's Disease
- ROSMAP: Religious Orders Study and Rush Memory and Aging Project
- MSBB: Mount Sinai Brain Bank
- MAYO: Mayo RNA-seq Study
- FDA: Food and Drug Administration
- ML: Machine Learning
- GABA: Gamma-Aminobutyric Acid
- NMDA: N-Methyl-D-Aspartate
- IRB: Institutional Review Board
- AUC: Area Under the Curve
- CI: Confidence Interval
- ROCAUC: Receiver Operating Characteristic Area Under the Curve
- Ca^{2+}: Calcium Ion
- ACC: Anterior Cingulate Cortex
- CBE: Cerebellum
- DLFPC: Dorsolateral Prefrontal Cortex
- FP: Frontal Pole
- IFG: Inferior Frontal Gyrus
- PCC: Posterior Cingulate Cortex

- PHG: Parahippocampal Gyrus
- STG: Superior Temporal Gyrus
- TCX: Temporal Cortex

Ethics approval and consent to participate

The use of electronic health record (EHR) data for the pharmacoepidemiologic analysis was reviewed by the Indiana University Institutional Review Board (IRB), which designated the study as exempt from further review (no human subjects research). The dataset—Optum's de-identified Clinformatics Data Mart Database—contains fully de-identified administrative claims for large commercial and Medicare Advantage health plan members, and informed consent was not required because all patient identifiers were removed prior to data access. Permission to use and analyze the de-identified dataset was obtained from the data provider. No additional consent to participate was needed for this secondary analysis of existing de-identified data. This study complies with ethical standards for retrospective analysis of de-identified data as per the Declaration of Helsinki.

Availability of data and materials

Bulk RNA sequencing datasets of ROSMAP, MSBB, and MAYO cohorts can be accessed with consent via the AD Knowledge Portal (https://adknowledgeportal.org; accession No. syn21241740) (9). Genomics datasets can be accessed via the AD Knowledge Portal (accession No. syn22264775). Optum's de-identified Clinformatics® Data Mart Database is not publicly available (accessibility can be obtained from Optum: https://www.optum.com/en/).

Competing interests

The authors declare that they have no competing interests.

Funding

This project has been funded by the National Institute of General Medical Sciences of the National Institute of Health (R01GM122845), the National Institute on Aging of the National Institute of Health (R01AG057555, R21AG083302), and the National Science Foundation (2226183).

Authors' contributions

M.M. prepared data, implemented the algorithms, performed the experiments, analyzed data, and wrote the manuscript; P.Z. performed EHR data mining, and wrote the manuscript; L. X. conceived and planned the experiments, and wrote the manuscript.

Acknowledgements

The authors acknowledge the important contributions of three publicly available datasets, including the ROSMAP, the Mount Sinai Brain Bank, and the MAYO. We thank the participants of the ROS, MAP, Mount Sinai Brain Bank, and Mayo for their time and participation.

Supplementary Files

1. Supplementary Table 1

Title: Subtissue-Specific Summary Statistics, Biomarker Sets, Genetic Drivers, and Bottleneck Genes.

Description: This file contains the complete lists of identified subtissue-level biomarkers, genetic variants (SNPs), genetic drivers and hub genes identified via Random Forest/SHAP and network analysis, along with their frequencies and summary statistics in each of the 36 subtissues.

2. Supplementary Table 2

Title: Demographic and Clinical Characteristics of the Pharmacoepidemiologic Cohort.

Description: This file provides comprehensive demographic and clinical profiles of the study population (N=364,733) stratified by promethazine (N=353,856) and cyproheptadine (N=10,877) exposure. It includes distributions of age, sex, race, comorbidities (e.g., cardiovascular, metabolic, and neurological conditions), and index year categories. These data underpin the baseline characteristics and covariate adjustments used in the Cox proportional hazards models to assess promethazine's association with reduced Alzheimer's disease risk.

3. Supplementary Table 3

Title: Covariate-adjusted Cox Model Full results: Associations with Alzheimer's Disease.

Description: This file details the complete results of the covariate-adjusted Cox proportional hazards regression analysis, including hazard ratios (HRs), 95% confidence intervals (CIs), and p-values for promethazine exposure and all confounders (e.g., age, comorbidities, and temporal factors). Key findings include the significant inverse association between promethazine use and Alzheimer's disease incidence (HR = 0.38, 95% CI: 0.27–0.53; $p < 0.001$), alongside adjustments for covariates such as age ≥75 (HR = 8.96) and neurological/psychiatric comorbidities. These data underlie the statistical findings presented in the Results section of the main manuscript, offering transparency into the modeling approaches and key risk estimates.

References

1. Monteiro AR, Barbosa DJ, Remião F, Silva R. Alzheimer's disease: Insights and new prospects in disease pathophysiology, biomarkers and disease-modifying drugs. Biochem Pharmacol. 2023 May 1;211:115522.

2. Zhang J, Zhang Y, Wang J, Xia Y, Zhang J, Chen L. Recent advances in Alzheimer's disease: mechanisms, clinical trials and new drug development strategies. Signal Transduct Target Ther [Internet]. 2024;9(1):211. Available from: https://doi.org/10.1038/s41392-024-01911-3

3. De A, Mishra TK, Saraf S, Tripathy B, Reddy SS. A Review on the Use of Modern Computational Methods in Alzheimer's Disease-Detection and Prediction. Curr Alzheimer Res [Internet]. 2024 Mar 12 [cited 2025 Jan 12];20(12):845–61. Available from: https://pubmed.ncbi.nlm.nih.gov/38468529/

4. Young AL, Oxtoby NP, Garbarino S, Fox NC, Barkhof F, Schott JM, et al. Data-driven modelling of neurodegenerative disease progression: thinking outside the black box. Nat Rev Neurosci [Internet]. 2024 Feb 1 [cited 2025 Jan 12];25(2):111–30. Available from: https://pubmed.ncbi.nlm.nih.gov/38191721/

5. Lundberg SM, Lee SI. A Unified Approach to Interpreting Model Predictions. Adv Neural Inf Process Syst [Internet]. 2017 May 22 [cited 2025 Jan 12];2017-December:4766–75. Available from: https://arxiv.org/abs/1705.07874v2

6. De Jager PL, Ma Y, McCabe C, Xu J, Vardarajan BN, Felsky D, et al. A multi-omic atlas of the human frontal cortex for aging and Alzheimer's disease research. Scientific Data 2018 5:1 [Internet]. 2018 Aug 7 [cited 2025 Jan 12];5(1):1–13. Available from: https://www.nature.com/articles/sdata2018142

7. Wang M, Beckmann ND, Roussos P, Wang E, Zhou X, Wang Q, et al. The Mount Sinai cohort of large-scale genomic, transcriptomic and proteomic data in Alzheimer's disease. Scientific Data 2018 5:1 [Internet]. 2018 Sep 11 [cited 2025 Jan 12];5(1):1–16. Available from: https://www.nature.com/articles/sdata2018185

8. Allen M, Carrasquillo MM, Funk C, Heavner BD, Zou F, Younkin CS, et al. Human whole genome genotype and transcriptome data for Alzheimer's and other neurodegenerative diseases. Scientific Data 2016 3:1 [Internet]. 2016 Oct 11 [cited 2025 Jan 12];3(1):1–10. Available from: https://www.nature.com/articles/sdata201689

9. Hodes RJ, Buckholtz N. Accelerating Medicines Partnership: Alzheimer's Disease (AMP-AD) Knowledge Portal Aids Alzheimer's Drug Discovery through Open Data Sharing. Expert Opin Ther Targets [Internet]. 2016 Apr 2 [cited 2025 Jan 12];20(4):389–91. Available from: https://pubmed.ncbi.nlm.nih.gov/26853544/

10. Pedregosa FABIANPEDREGOSA F, Michel V, Grisel OLIVIERGRISEL O, Blondel M, Prettenhofer P, Weiss R, et al. Scikit-learn: Machine Learning in Python. The Journal of

Machine Learning Research [Internet]. 2011 Nov 1 [cited 2025 Jan 13];12:2825–30. Available from: https://dl.acm.org/doi/10.5555/1953048.2078195

11. Lundberg SM, Erion G, Chen H, DeGrave A, Prutkin JM, Nair B, et al. From local explanations to global understanding with explainable AI for trees. Nature Machine Intelligence 2020 2:1 [Internet]. 2020 Jan 17 [cited 2025 Jan 13];2(1):56–67. Available from: https://www.nature.com/articles/s42256-019-0138-9

12. Andrade-Guerrero J, Santiago-Balmaseda A, Jeronimo-Aguilar P, Vargas-Rodríguez I, Cadena-Suárez AR, Sánchez-Garibay C, et al. Alzheimer's Disease: An Updated Overview of Its Genetics. Int J Mol Sci [Internet]. 2023 Feb 1 [cited 2025 Jan 12];24(4):3754. Available from: https://pmc.ncbi.nlm.nih.gov/articles/PMC9966419/

13. Ritchie ME, Phipson B, Wu D, Hu Y, Law CW, Shi W, et al. limma powers differential expression analyses for RNA-sequencing and microarray studies. Nucleic Acids Res [Internet]. 2015 Apr 20 [cited 2025 Jan 12];43(7):e47–e47. Available from: https://dx.doi.org/10.1093/nar/gkv007

14. Sherman BT, Hao M, Qiu J, Jiao X, Baseler MW, Lane HC, et al. DAVID: a web server for functional enrichment analysis and functional annotation of gene lists (2021 update). Nucleic Acids Res [Internet]. 2022 Jul 5 [cited 2025 Jan 12];50(W1):W216–21. Available from: https://pubmed.ncbi.nlm.nih.gov/35325185/

15. Langfelder P, Horvath S. Fast R Functions for Robust Correlations and Hierarchical Clustering. J Stat Softw [Internet]. 2012 Mar 7 [cited 2025 Jan 12];46(11):1–17. Available from: https://www.jstatsoft.org/index.php/jss/article/view/v046i11

16. Szklarczyk D, Kirsch R, Koutrouli M, Nastou K, Mehryary F, Hachilif R, et al. The STRING database in 2023: protein-protein association networks and functional enrichment analyses for any sequenced genome of interest. Nucleic Acids Res [Internet]. 2023 Jan 6 [cited 2025 Jan 12];51(D1):D638–46. Available from: https://pubmed.ncbi.nlm.nih.gov/36370105/

17. Bastian M, Heymann S, Jacomy M. Gephi: An Open Source Software for Exploring and Manipulating Networks. Proceedings of the International AAAI Conference on Web and Social Media [Internet]. 2009 Mar 19 [cited 2025 Jan 13];3(1):361–2. Available from: https://ojs.aaai.org/index.php/ICWSM/article/view/13937

18. Fernández-Torras A, Duran-Frigola M, Bertoni M, Locatelli M, Aloy P. Integrating and formatting biomedical data as pre-calculated knowledge graph embeddings in the Bioteque. Nature Communications 2022 13:1 [Internet]. 2022 Sep 9 [cited 2025 Jan 12];13(1):1–18. Available from: https://www.nature.com/articles/s41467-022-33026-0

19. Kalpaklioglu F, Baccioglu A. Efficacy and safety of H1-antihistamines: an update. Antiinflamm Antiallergy Agents Med Chem [Internet]. 2012 Jan 11 [cited 2025 Jan 12];11(3):230–7. Available from: https://pubmed.ncbi.nlm.nih.gov/23173575/

20. Harding Z, Wilkinson T, Stevenson A, Horrocks S, Ly A, Schnier C, et al. Identifying Parkinson's disease and parkinsonism cases using routinely collected healthcare data: A systematic review. PLoS One [Internet]. 2019 Jan 1 [cited 2025 Jan 12];14(1). Available from: https://pubmed.ncbi.nlm.nih.gov/30703084/

21. Wilkinson T, Ly A, Schnier C, Rannikmäe K, Bush K, Brayne C, et al. Identifying dementia cases with routinely collected health data: A systematic review. Alzheimer's & Dementia [Internet]. 2018 Aug 1 [cited 2025 Jan 12];14(8):1038. Available from: https://pmc.ncbi.nlm.nih.gov/articles/PMC6105076/

22. Cheng D, Dumontier C, Yildirim C, Charest B, Hawley CE, Zhuo M, et al. Updating and Validating the U.S. Veterans Affairs Frailty Index: Transitioning From ICD-9 to ICD-10. J Gerontol A Biol Sci Med Sci [Internet]. 2021 Jul 1 [cited 2025 Jan 12];76(7):1318–25. Available from: https://pubmed.ncbi.nlm.nih.gov/33693638/

23. Anwar MM, Özkan E, Gürsoy-Özdemir Y. The role of extracellular matrix alterations in mediating astrocyte damage and pericyte dysfunction in Alzheimer's disease: A comprehensive review. Eur J Neurosci [Internet]. 2022 Nov 1 [cited 2025 Jan 12];56(9):5453–75. Available from: https://pubmed.ncbi.nlm.nih.gov/34182602/

24. Griffiths J, Grant SGN. Synapse pathology in Alzheimer's disease. Semin Cell Dev Biol [Internet]. 2023 Apr 1 [cited 2025 Jan 12];139:13–23. Available from: https://pubmed.ncbi.nlm.nih.gov/35690535/

25. Kumari S, Dhapola R, Reddy DHK. Apoptosis in Alzheimer's disease: insight into the signaling pathways and therapeutic avenues. Apoptosis [Internet]. 2023 Aug 1 [cited 2025 Feb 27];28(7–8):943–57. Available from: https://pubmed.ncbi.nlm.nih.gov/37186274/

26. Yao J, He Z, You G, Liu Q, Li N. The Deficits of Insulin Signal in Alzheimer's Disease and the Mechanisms of Vanadium Compounds in Curing AD. Curr Issues Mol Biol [Internet]. 2023 Aug 1 [cited 2025 Feb 27];45(8):6365–82. Available from: https://pubmed.ncbi.nlm.nih.gov/37623221/

27. Georgieva I, Tchekalarova J, Iliev D, Tzoneva R. Endothelial Senescence and Its Impact on Angiogenesis in Alzheimer's Disease. Int J Mol Sci [Internet]. 2023 Jul 1 [cited 2025 Jan 12];24(14). Available from: https://pubmed.ncbi.nlm.nih.gov/37511104/

28. Ramezani M, Fernando M, Eslick S, Asih PR, Shadfar S, Bandara EMS, et al. Ketone bodies mediate alterations in brain energy metabolism and biomarkers of Alzheimer's disease. Front Neurosci [Internet]. 2023 [cited 2025 Jan 12];17. Available from: https://pubmed.ncbi.nlm.nih.gov/38033541/

29. Fabiani C, Antollini SS. Alzheimer's Disease as a Membrane Disorder: Spatial Cross-Talk Among Beta-Amyloid Peptides, Nicotinic Acetylcholine Receptors and Lipid Rafts. Front Cell Neurosci [Internet]. 2019 Jul 16 [cited 2025 Jan 12];13. Available from: https://pubmed.ncbi.nlm.nih.gov/31379503/

30. Thakur S, Dhapola R, Sarma P, Medhi B, Reddy DHK. Neuroinflammation in Alzheimer's Disease: Current Progress in Molecular Signaling and Therapeutics. Inflammation [Internet]. 2023 Feb 1 [cited 2025 Jan 12];46(1):1–17. Available from: https://pubmed.ncbi.nlm.nih.gov/35986874/

31. Pelucchi S, Stringhi R, Marcello E. Dendritic Spines in Alzheimer's Disease: How the Actin Cytoskeleton Contributes to Synaptic Failure. Int J Mol Sci [Internet]. 2020 Feb 1 [cited 2025 Jan 12];21(3). Available from: https://pubmed.ncbi.nlm.nih.gov/32019166/

32. Le CK, Stevens CA, Park JH, Clark RF. Promethazine: A Review of Therapeutic Uses and Toxicity. J Emerg Med [Internet]. 2024 Oct 9 [cited 2025 Jan 12]; Available from: https://linkinghub.elsevier.com/retrieve/pii/S0736467924003251

33. Huf G, Alexander J, Gandhi P, Allen MH. Haloperidol plus promethazine for psychosis-induced aggression. Cochrane Database Syst Rev [Internet]. 2016 Nov 25 [cited 2025 Jan 12];11(11). Available from: https://pubmed.ncbi.nlm.nih.gov/27885664/

34. Bai L, Li F. To explore the protective mechanism of promethazine against hippocampal neuron injury based on network pharmacology and experimental verification. Medicine [Internet]. 2024 Dec 6 [cited 2025 Mar 12];103(49):e40550. Available from: https://pubmed.ncbi.nlm.nih.gov/39654167/

35. McClure RA, Chumbley CW, Reyzer ML, Wilson K, Caprioli RM, Gore JC, et al. Identification of promethazine as an amyloid-binding molecule using a fluorescence high-throughput assay and MALDI imaging mass spectrometry. Neuroimage Clin [Internet]. 2013 [cited 2025 Mar 12];2(1):620. Available from: https://pmc.ncbi.nlm.nih.gov/articles/PMC3778261/

36. Corriveau S, Heydari B, Garceau P. Does Disopyramide Still Have a Place in the Management of Obstructive Hypertrophic Cardiomyopathy? CJC Open. 2024 Jun 1;6(6):811–7.

37. Barbieri R, Nizzari M, Zanardi I, Pusch M, Gavazzo P. Voltage-Gated Sodium Channel Dysfunctions in Neurological Disorders. Life (Basel) [Internet]. 2023 May 1 [cited 2025 Mar 12];13(5). Available from: https://pubmed.ncbi.nlm.nih.gov/37240836/

38. Browder E, Kapp S, Ange-van Heugten K, Flowers J, Christian LS, Dombrowski DS. The Effect of Pyrantel Pamoate Treatment on Fecal Pinworm (Leidynema appendiculata) Parasites of Dietary Dubia Roaches (Blaptica dubia): Efforts to Eliminate Passthrough Fecal Pseudoparasites in Lesser Hedgehog Tenrecs (Echinops telfairi). Journal of Zoological and Botanical Gardens 2023, Vol 4, Pages 146-157 [Internet]. 2023 Feb 10 [cited 2025 Jan 12];4(1):146–57. Available from: https://www.mdpi.com/2673-5636/4/1/15/htm

39. Mitra S, Khatri SN, Maulik M, Bult-Ito A, Schulte M. Allosterism of Nicotinic Acetylcholine Receptors: Therapeutic Potential for Neuroinflammation Underlying Brain

Trauma and Degenerative Disorders. Int J Mol Sci [Internet]. 2020 Jul 2 [cited 2025 Mar 12];21(14):4918. Available from: https://pmc.ncbi.nlm.nih.gov/articles/PMC7404387/

40. Hao F, Yin S, Tang L, Zhang X, Zhang S. Nicardipine versus Labetalol for Hypertension during Acute Stroke: A Systematic Review and Meta-Analysis. Neurol India [Internet]. 2022 [cited 2025 Jan 12];70(5):1793–9. Available from: https://pubmed.ncbi.nlm.nih.gov/36352567/

41. Huang BR, Chang PC, Yeh WL, Lee CH, Tsai CF, Lin C, et al. Anti-Neuroinflammatory Effects of the Calcium Channel Blocker Nicardipine on Microglial Cells: Implications for Neuroprotection. PLoS One [Internet]. 2014 Mar 12 [cited 2025 Mar 12];9(3):e91167. Available from: https://pmc.ncbi.nlm.nih.gov/articles/PMC3951295/

42. Lovell MA, Abner E, Kryscio R, Xu L, Fister SX, Lynn BC. Calcium Channel Blockers, Progression to Dementia, and Effects on Amyloid Beta Peptide Production. Oxid Med Cell Longev [Internet]. 2015 [cited 2025 Mar 12];2015:787805. Available from: https://pmc.ncbi.nlm.nih.gov/articles/PMC4499419/

43. Duncombe J, Kitamura A, Hase Y, Ihara M, Kalaria RN, Horsburgh K. Chronic cerebral hypoperfusion: a key mechanism leading to vascular cognitive impairment and dementia. Closing the translational gap between rodent models and human vascular cognitive impairment and dementia. Clin Sci (Lond) [Internet]. 2017 Oct 1 [cited 2025 Mar 12];131(19):2451–68. Available from: https://pubmed.ncbi.nlm.nih.gov/28963120/

44. De Wit H, Vicini L, Haig GM, Hunt T, Feltner D. Evaluation of the abuse potential of pagoclone, a partial GABAA agonist. J Clin Psychopharmacol [Internet]. 2006 Jun [cited 2025 Jan 12];26(3):268–73. Available from: https://pubmed.ncbi.nlm.nih.gov/16702891/

45. Caveney AF, Giordani B, Haig GM. Preliminary effects of pagoclone, a partial GABAA agonist, on neuropsychological performance. Neuropsychiatr Dis Treat [Internet]. 2008 [cited 2025 Mar 12];4(1):277. Available from: https://pmc.ncbi.nlm.nih.gov/articles/PMC2515892/

46. Lee YT, Tan YJ, Oon CE. Benzimidazole and its derivatives as cancer therapeutics: The potential role from traditional to precision medicine. Acta Pharm Sin B [Internet]. 2022 Feb 1 [cited 2025 Jan 12];13(2):478. Available from: https://pmc.ncbi.nlm.nih.gov/articles/PMC9978992/

47. Mayer AMS, Hall ML, Lynch SM, Gunasekera SP, Sennett SH, Pomponi SA. Differential modulation of microglia superoxide anion and thromboxane B2 generation by the marine manzamines. BMC Pharmacol [Internet]. 2005 Mar 11 [cited 2025 Mar 12];5:6. Available from: https://pmc.ncbi.nlm.nih.gov/articles/PMC1079881/

48. LK B, AB W, A S, HS W. Astrocytic glycogen metabolism in the healthy and diseased brain. J Biol Chem [Internet]. 2018 May 11 [cited 2025 Mar 12];293(19):7108–16. Available from: https://pubmed.ncbi.nlm.nih.gov/29572349/

49. Lee KY, Rhodes JS, Saif MTA. Astrocyte-mediated Transduction of Muscle Fiber Contractions Synchronizes Hippocampal Neuronal Network Development. Neuroscience [Internet]. 2023 Apr 1 [cited 2025 Mar 12];515:25–36. Available from: https://pubmed.ncbi.nlm.nih.gov/36736611/

50. Villa C, Combi R. Epigenetics in Alzheimer's Disease: A Critical Overview. Int J Mol Sci [Internet]. 2024 Jun 1 [cited 2025 Mar 12];25(11). Available from: https://pubmed.ncbi.nlm.nih.gov/38892155/

51. Crossley CA, Rajani V, Yuan Q. Modulation of L-type calcium channels in Alzheimer's disease: A potential therapeutic target. Comput Struct Biotechnol J [Internet]. 2022 Jan 1 [cited 2025 Mar 12];21:11–20. Available from: https://pubmed.ncbi.nlm.nih.gov/36514335/

52. Grubman A, Chew G, Ouyang JF, Sun G, Choo XY, McLean C, et al. A single-cell atlas of entorhinal cortex from individuals with Alzheimer's disease reveals cell-type-specific gene expression regulation. Nat Neurosci [Internet]. 2019 Dec 1 [cited 2025 Jan 12];22(12):2087–97. Available from: https://pubmed.ncbi.nlm.nih.gov/31768052/

53. Rai D, Zhou Y, Feng S, Saparov A, Yao Z. A Practical Review of Mechanistic Interpretability for Transformer-Based Language Models. 2024 Jul 2 [cited 2025 Jan 12]; Available from: http://arxiv.org/abs/2407.02646